

Mass of Abrikosov vortex in high-temperature superconductor $\text{YBa}_2\text{Cu}_3\text{O}_{7-\delta}$

Roman Tesař^{1,*}, Michal Šindler¹, Christelle Kadlec¹, Pavel Lipavský², Ladislav Skrbek², and Jan Koláček¹

¹Institute of Physics, Czech Academy of Sciences, Na Slovance 2, 182 21 Prague 8, Czech Republic

²Faculty of Mathematics and Physics, Charles University, Ke Karlovu 3, 121 16 Prague 2, Czech Republic

*tesar@fzu.cz

ABSTRACT

Mass of Abrikosov vortices defied experimental observation for more than four decades. We demonstrate a method of its detection in high-temperature superconductors. Similarly to electrons, fluxons circulate in the direction given by the magnetic field, causing circular dichroism. We report the magneto-transmittance of a nearly optimally doped thin $\text{YBa}_2\text{Cu}_3\text{O}_{7-\delta}$ film, measured using circularly polarized submillimeter waves. The circular dichroism emerges in the superconducting state and increases with dropping temperature. Our results confirm the dominant role of quasiparticle states in the vortex core and yield the diagonal fluxon mass of 2.2×10^8 electron masses per centimeter at 45 K and zero-frequency limit and even larger off-diagonal mass of $4.9 \times 10^8 m_e/\text{cm}$.

The limitations of today's digital technology will likely be overcome by ultra-fast superconductive electronics¹, quantum circuits², and quantum information processing. Such advanced electronic devices can operate within the framework of *fluxonics* taking advantage of intrinsic properties of superconducting vortices. Abrikosov vortices, or fluxons, are ideal information carriers: they are topologically stable and keep a uniform nano-scale size given by quantum conditions.^{3,4}

Nevertheless, the fluxon mass is a particularly controversial issue. Its theoretical estimates are scattered over more than eight orders of magnitude. Vortex mass in superconductors has been debated for over 50 years since its theoretical prediction by Suhl⁵, $4000 m_e/\text{cm}$ for Nb, where m_e is the electron mass. Multiple theories emerged in 1991, stimulated by the discovery of high- T_c superconductors; for instance, the vortex mass in YBaCuO was predicted⁶ to reach $10^8 m_e/\text{cm}$. Rather different trends follow from the theory of Han *et al.*⁷, which gives $10^{13} m_e/\text{cm}$ in Nb at 5 K, while for YBaCuO at the same temperature, it yields $3 \times 10^9 m_e/\text{cm}$. Additionally, the vortex mass can be increased by backflow effects⁸ or by the strain field^{9,10} with estimates for YBaCuO from dominant 10^{10} to negligible $10^4 m_e/\text{cm}$. We also note that theories for the mass of quantized vortices in closely related superfluids offer similarly conflicting results^{11,12} that span the full range from the infinite mass^{13,14} to the negligible one¹⁵.

In contrast to the plethora of theoretical predictions of the effective vortex mass in type-II superconductors, we are aware of only two relevant experiments, both supporting rather large values. Fil *et al.*¹⁶ measured the acousto-electric effect in YB_6 and deduced a vortex mass of $10^{10} m_e/\text{cm}$. Golubchik *et al.*¹⁷ observed the movement of individual vortices in a superconducting Nb film near its critical temperature by combining high-resolution magneto-optical imaging with ultrafast heating and cooling. A nonzero mass is indispensable to explain their data; they estimated the fluxon mass to be in interval $(0.3 - 6) \times 10^8 m_e/\text{cm}$.

The extremely large spread in theoretically predicted values and scarce experimental data available motivated us to independently determine the mass of a fluxon. Here, we present relevant experiments leading to the evaluation of the vortex mass in nearly optimally doped $\text{YBa}_2\text{Cu}_3\text{O}_{7-\delta}$. Our approach is inspired by the cyclotron resonance measurement, a method commonly employed to obtain the effective mass of charge carriers in semiconductors. Exposed to an external magnetic field, charged particles move in circular orbits and, under certain conditions, resonantly absorb monochromatic radiation. In the case of fluxons, however, the cyclotron motion is induced by an interaction with circularly polarized far-infrared laser light. This interaction depends on the sense of circular polarization and manifests itself as a differential transmittance for clockwise and anti-clockwise polarized waves, known as magnetic circular dichroism. We show that the theory of Kopnin and coworkers reproduces our experimental data *without any fitting parameter*. Thus, our results support the theory of the fluxon mass developed by Kopnin and Vinokur¹⁸ and that of the Magnus force reduction by the factor of Kopnin and Kravtsov¹⁹.

Far-infrared measurements of the fluxon mass

Magneto-transmittance of circularly polarized light

We designed and developed a unique far-infrared (FIR) transmission experiment capable of probing the circular dichroism (see Fig. 1). The breakthrough that has eventually allowed us to conduct this research is a custom-made retarder²⁰ inserted in the optical path near the FIR-laser output aperture; it delays the horizontal polarization relative to the vertical one by an adjustable phase difference. A mutual phase shift of $\pm\pi/2$ converts the THz beam of equal vertical and horizontal polarization components into the circularly polarized state. Since the phase delay introduced by the retarder is inversely proportional to the wavelength of the incoming light, each laser line requires a separate adjustment.

We measured the transmittance of the sample for several laser lines at wavelengths 119, 163, 312, 419, and 433 μm ²¹, corresponding to the terahertz circular frequencies ω of 15.9, 11.6, 6.05, 4.50, and 4.35×10^{12} rad/s, respectively. Our setup shown in Fig. 1a enables fast flips between clockwise (+) and anti-clockwise (−) circular polarizations, consequently, we probed the transmittance \mathcal{T}_+ and \mathcal{T}_- of both polarizations under identical conditions. The transmittance, i.e., the fraction of laser energy transmitted through the sample, is evaluated as the bolometer-to-pyrodetector signal ratio, effectively eliminating any possible time instability in the laser power. Identical profiles of both signals confirm that the transmittance is measured in the linear regime.

Our experimental protocol is as follows: in experimental runs, we apply a magnetic field at a temperature well above T_c . As the temperature drops, vortices freeze into a regular Abrikosov lattice. The applied magnetic field B is kept constant since any change in B would result in inhomogeneous patterns of the vortex density. The temperature T is swept down and up at a steady sweep rate of 2.5 K/min, the instantaneous temperature of the sample being recorded together with the transmittance. Care is taken that the down and up sweeps do not show any hysteresis.

Fig. 1c displays a typical temperature behavior of the transmittance observed in the external magnetic field of 10 T using a 312 μm laser line. The results obtained with different laser lines are similar. As expected, the transmittance measured in zero field does not show any dichroism, in absence of Abrikosov vortices to induce an asymmetry. In nonzero fields, however, the low-temperature circular dichroism is clearly observed and can be attributed to the formation of vortices threading the sample. The effect is enhanced in higher applied magnetic fields, thanks to the growing areal density of Abrikosov vortices (see Fig. 1d). We focus on the low-temperature region, $T < 50$ K, where the thermal quasiparticles play a negligible role and the response of the system is fully governed by the motion of fluxons.

Sample specification by time-domain terahertz spectroscopy

We chose the most common high- T_c material $\text{YBa}_2\text{Cu}_3\text{O}_{7-\delta}$ in the form of a thin film with a thickness of $L = 107$ nm, and with CuO_2 planes parallel to the surface. The sample was prepared at National Chiao Tung University (Taiwan) using a pulsed laser deposition method from a stoichiometric target on a lanthanum aluminate substrate oriented in the (100) plane. The substrate dimensions are $10 \times 10 \times 0.5$ mm³. Several measurements were performed to establish sample properties. Figure 2 summarizes some relevant results.

The critical temperature of the film, $T_c = 87.6$ K, was determined from a dedicated measurement of dc resistivity ρ (Fig. 2a). For our slightly underdoped sample, this T_c corresponds to the hole density²² $n_0 = 1.68 \times 10^{27}/\text{m}^3$. The linear slope of ρ extrapolated to zero temperature shows negligible residual resistivity, so that the relaxation time is inversely proportional to temperature.

Additional film properties were established in a separate experiment using standard time-domain THz spectroscopy. Broadband linearly polarized THz pulses (0.3–2.5 THz) were generated by exciting an interdigitated LT-GaAs emitter with a Ti:sapphire femtosecond laser beam at 800 nm²³. We measured the complex conductivity $\sigma = \sigma' + i\sigma''$ for frequencies $\omega/2\pi$ in the range 0.5–2 THz at temperatures from 4 to 100 K (Figs. 2b,d,e). At the zero magnetic field and below T_c , the two-fluid model fit confirms the dominant London contribution, $\sigma_0 \approx ine^2/(m\omega)$, with a temperature-dependent condensate density $n = n_0(1 - T^4/T_c^4)$, the hole mass $m = 3.3 m_e$, and the elementary charge e . Comparing the conductivities at temperatures of 4 K and $T_N = 100$ K in Fig. 2d, we found the relaxation time $\tau_N = 5 \times 10^{-14}$ s. Conductivities at all temperatures from 4 to 100 K are consistent with $\tau = \tau_N T_N/T$.

Our sample is moderately clean. Its purity is given by the lifetime measured on the energy scale¹⁸ as $k_B^2 T_c^2 \tau / \hbar E_F$, where k_B is the Boltzmann constant and \hbar is the reduced Planck constant. The Fermi energy $E_F = \hbar^2 k_F^2 / 2m$ depends on the hole doping. For the hole density of our sample, the Fermi surface is cylindrical rather than spherical, and the Fermi momentum follows from the 2D density of holes in the CuO_2 plane $n_{2D} = n_0 c / 2 = k_F^2 / (2\pi)$, where $c = 11.68$ Å is the YBaCuO lattice parameter in the z -direction. The resulting Fermi energy $E_F = 71$ meV yields the value of $k_B^2 T_c^2 \tau / \hbar E_F \sim 0.1$, corresponding to the moderately clean sample.

According to Kopnin and Vinokur¹⁸, the moderately clean d-wave superconductor behaves as the s-wave one. In the absence of reliable formulas for angular frequency ω_0 of quasiparticles bounded in the vortex core in the d-wave superconductors, we used $\hbar\omega_0 = (\Delta_0/k_F\xi_0)(1 - T^2/T_c^2)$ for the conventional superconductors²⁴. We deduced the coherence length ξ_0 from the upper critical field in the zero-temperature limit²⁵, $B_{c2} = 122 \text{ T} = \Phi_0/2\pi\xi_0^2$, where Φ_0 is the magnetic flux quantum. From the energy gap $2\Delta_0 = 4.3k_B T_c$, we obtained $\omega_0 = 4.4 \times 10^{12} \text{ rad/s}$, a value close to $4.5 \times 10^{12} \text{ rad/s}$ of our 419 μm laser line.

To complete the sample characteristics, we assume pinning of vortices by layer imperfections, for example, the surface roughness. Figure 2e shows the conductivity in the magnetic field of 7 T applied perpendicularly to the film^{26,27}. It was interpreted either with the theory specified below or with the model used by Parks²⁸, both indicating that the vortex pinning is rather weak with the Labusch coefficient $\kappa \approx 2 \times 10^5 \text{ N/m}^2$.

Theoretical prediction

Our aim is to compare experimental values of $\mathcal{T}_+/\mathcal{T}_-$ with a theoretical model. Using the above sample parameters, we can evaluate the film conductivity σ_{\pm} from which the transmittance \mathcal{T}_{\pm} results. The theoretical prediction shown in Fig. 3 is based on the Yeh formalism²⁹ and covers interferences in the weakly birefringent substrate. For the purpose of discussion, we refer to an approximation $\mathcal{T}_+/\mathcal{T}_- = |\sigma_-|^2/|\sigma_+|^2$ which differs from the exact theory by less than 4% as shown in the Supplementary Information³⁰.

Kopnin and Vinokur³¹ provided the theoretical conductivities σ_{\pm} derived under very general conditions. Our study allows for two simplifications. First, we focus on temperatures about 45 K, where we observe a large dichroic signal. At such low temperatures, extended quasiparticles are very dilute so that we can neglect their contribution to the electric current \mathbf{J} as well as their effect on vortices. Second, the cyclotron frequency $\omega_c = eB/m$ is small on the scale of the quasiparticle lifetime, $\omega_c\tau \ll 1$ for all experimental magnetic fields, which simplifies dynamics of quasiparticles in the vortex core. Under these conditions, the equation of motion for a fluxon of unitary length takes the form of Newton's law³¹

$$\dot{\mathbf{p}} = \mathbf{F} + \pi\hbar n[(\mathbf{J}/(en) - \mathbf{v}) \times \mathbf{z}] - \kappa\mathbf{u} \quad (1)$$

with the time derivative of momentum \mathbf{p} and the force \mathbf{F} from the interaction of the vortex core with the crystal lattice. Unlike Kopnin and Vinokur, we include the pinning force with the Labusch parameter κ and vortex displacement \mathbf{u} related to its velocity as $\dot{\mathbf{u}} = \mathbf{v}$. The Magnus force, given by the vector product of the magnetic field direction $\mathbf{z} = \mathbf{B}/B$ and the vortex velocity related to the condensate current, covers a force by which the flowing condensate acts on the fluxon.

In Kopnin's model, the fluxon momentum \mathbf{p} is a total momentum of quasiparticles in the vortex core which rotate about the vortex axis at an angular frequency ω_0 . For our moderately clean sample, the fluxon momentum at the low-temperature limit depends on its velocity as¹⁸ $\mathbf{p} = \mu_{\parallel}\mathbf{v} - \mu_{\perp}[\mathbf{v} \times \mathbf{z}]$, where

$$\mu_{\parallel} = \pi\hbar n \frac{\omega_0\tau^2}{(1 - i\omega\tau)^2 + \omega_0^2\tau^2} \quad \text{and} \quad \mu_{\perp} = \pi\hbar n\tau \frac{1 - i\omega\tau}{(1 - i\omega\tau)^2 + \omega_0^2\tau^2}. \quad (2)$$

The diagonal mass μ_{\parallel} is complex at finite frequencies, which reflects a delay between a change of the vortex velocity and a change of the total momentum of quasiparticles in its core. The off-diagonal mass μ_{\perp} describes a property common in anisotropic systems that the velocity of an excitation is not parallel with its momentum.

Quasiparticles disturbed by the vortex motion and action of the FIR light eventually lose their momentum in collisions with impurities and phonons. Via these collisions, the crystal lattice acts on the fluxon by force \mathbf{F} . With the collision integral approximated by a single relaxation time τ , the force and the momentum are simply related by $\mathbf{F} = -\dot{\mathbf{p}}/\tau$. The longitudinal force $-(\mu_{\parallel}/\tau)\mathbf{v}$ is a vortex friction. The transversal force $(\mu_{\perp}/\tau)[\mathbf{v} \times \mathbf{z}]$ reduces the Magnus force giving the Kopnin-Kravtsov force¹⁹ in the dc limit.

The electric field in the film³¹⁻³³

$$\mathbf{E} = \frac{1}{\sigma_0}\mathbf{J} - [\mathbf{v} \times \mathbf{B}] \quad (3)$$

has a skin component \mathbf{J}/σ_0 from the penetrating incident light, and an electric field $-[\mathbf{v} \times \mathbf{B}]$ generated by the vortex motion. At low frequencies, the London conductivity σ_0 diverges and the electric field achieves the dc form of the Josephson relation. In the absence of the magnetic field, Eq. (3) reduces to the London formula. Alternatively, one can employ the Coffey-Clem model used by Parks *et al.*²⁸, which is equivalent to Eq. (3).

Conductivities σ_{\pm} are diagonal elements of the conductivity tensor $\hat{\sigma}\mathbf{E} = \mathbf{J}$ in the helical basis. Eigen-vectors of circularly polarized light are constructed from basis vectors in the film plane, e.g., the electric field $\mathbf{E} = E_{\pm}e^{-i\omega t}\mathbf{e}_{\pm}$,

where $\mathbf{e}_{\pm} = (\mathbf{x} \pm is\mathbf{y})/\sqrt{2}$ are vectors of the helical basis and $s = \text{sign}(\mathbf{B} \cdot \mathbf{k})$ reflects the parallel or the anti-parallel orientation of the applied magnetic field \mathbf{B} with respect to the wavevector \mathbf{k} of incoming light. The eigen-vectors satisfy $[\mathbf{e}_{\pm} \times \mathbf{z}] = \pm is\mathbf{e}_{\pm}$, therefore, each of the vector equations (1) and (3) splits into two independent scalar equations for (+) and (-) polarizations. One can easily eliminate the velocity \mathbf{v} and write the conductivities

$$\frac{1}{\sigma_{\pm}} = \frac{E_{\pm}}{J_{\pm}} = \frac{1}{\sigma_0} + \frac{B}{en} \left(\frac{\omega_0\tau}{1 - i\omega\tau \mp is\omega_0\tau} + i\frac{\kappa}{\pi\hbar\omega n} \right)^{-1} \quad (4)$$

needed for the theoretical prediction of the transmittance.

Discussion

Experiment versus theoretical prediction

With the full set of sample parameters established from the time-domain spectroscopy, the simplified Kopnin-Vinokur conductivity (4) furnishes us with the theoretical prediction of the circular dichroism. Figure 3 compares this prediction and the experimentally observed dichroism for several values of the applied magnetic field and the THz-laser wavelength. The differences between theory and experiment are smaller than the experimental errors.

With increasing wavelength and field strength, the transmittance ratio $\mathcal{T}_+/\mathcal{T}_-$ gradually deviates from unity. The observed trends can be understood in terms of Eq. (3). The field dependence arises from the dominant London contribution $1/\sigma_0$ complemented by the Josephson-type resistivity, which is linear in \mathbf{B} . The variation with wavelength has a similar cause: for lower frequencies, the London resistivity $1/\sigma_0 \approx -i\omega m/(ne^2)$ is smaller so the Josephson part becomes dominant.

Vortex mass from experiment

Figure 3 documents that the theory of Kopnin and Vinokur is relevant for the THz dynamics of vortices. Since the observed frequency dependence of magneto-transmission agrees with the theoretical one, even with *no adjustable parameters*, the extrapolation of our results to low frequencies is justified. Based on this, we used their theory to find the vortex mass from our data.

While the sample parameters n , σ_0 , and τ are sound, κ and ω_0 are less clear. The Labusch parameter κ has a minor effect on the dichroism, therefore we kept the value $\kappa = 2 \times 10^5 \text{ N/m}^2$. The angular frequency ω_0 was established by the least-square fit of $\mathcal{T}_+/\mathcal{T}_-$ data. The best-fit value $\omega_0 = 4.3 \times 10^{12} \text{ rad/s}$ was very close to $4.4 \times 10^{12} \text{ rad/s}$ estimated above. We believe that such close agreement of observed and estimated frequency is fortuitous.

At THz frequencies, where the circular dichroism was found, both diagonal and off-diagonal masses are complex. They become real in the low-frequency limit, as apparent from Eq. (2). Using the experimentally established values of $\omega_0 = 4.3 \times 10^{12} \text{ rad/s}$ and other sample parameters, we evaluated the zero-frequency components of the fluxon mass. In $\text{YBa}_2\text{Cu}_3\text{O}_{7-\delta}$ at 45 K, the diagonal mass μ_{\parallel} amounts to $2.2 \times 10^8 m_e/\text{cm}$, while the off-diagonal mass μ_{\perp} is more than twice larger, $4.9 \times 10^8 m_e/\text{cm}$.

In summary, we have developed a reliable experimental method to measure the circular dichroism of superconducting films threaded by Abrikosov vortices. To interpret our data in terms of vortex dynamics, we have established all the essential material parameters from independent time-domain THz spectroscopy and dc-resistivity measurements. The observed dichroism is in good agreement with the theory of Kopnin and Vinokur based on the circular motion of quasiparticles in the vortex core. Their angular frequency was experimentally determined and used to extrapolate the vortex mass from THz frequencies to low-frequency motion.

References

1. S. Anders *et al.*, European roadmap on superconductive electronics – status and perspectives, *Physica C* **470**, 2079 (2010).
2. A. D. King *et al.*, Observation of topological phenomena in a programmable lattice of 1,800 qubits, *Nature* **560**, 456 (2018).
3. Golod, T., Iovan, A., and Krasnov, V. Single Abrikosov vortices as quantized information bits. *Nat Commun* **6**, 8628 (2015). <https://doi.org/10.1038/ncomms9628>
4. V. K. Vlasko-Vlasov, F. Colauto, T. Benseman, D. Rosenmann, and W.-K. Kwok Triode for Magnetic Flux Quanta. *Sci Rep* **6**, 36847 (2016). <https://doi.org/10.1038/srep36847>
5. H. Suhl, Inertial mass of a moving fluxoid, *Phys. Rev. Lett.* **14**, 226 (1965).

6. M. W. Coffey and Z. Hao, Dipolar electric field induced by a vortex moving in an anisotropic superconductor, *Phys. Rev. B* **44**, 5230 (1991).
7. J. H. Han, J. S. Kim, M. J. Kim, and P. Ao, Effective vortex mass from microscopic theory, *Phys. Rev. B* **71**, 125108 (2005).
8. E. B. Sonin, Transverse force on a vortex and vortex mass: Effects of free bulk and vortex-core bound quasiparticles, *Phys. Rev. B* **87**, 134515 (2013).
9. E. Šimánek, Inertial mass of a fluxon in a deformable superconductor, *Phys. Lett. A* **154**, 309 (1991).
10. M. W. Coffey, Deformable superconductor model for the fluxon mass, *Phys. Rev. B* **49**, 9774 (1994).
11. L. A. Toikka and J. Brand, Asymptotically solvable model for a solitonic vortex in a compressible superfluid, *New J. Phys.* **19**, 023029 (2017).
12. T. Simula, Vortex mass in a superfluid, *Phys. Rev. A* **97**, 023609 (2018).
13. V. N. Popov, Quantum vortices and phase-transition in bose systems, *Zh. Eksp. Teor. Fiz.* **64**, 672 (1973). [*Sov. Phys. JETP* **37**, 341 (1973)].
14. J. M. Duan, Mass of a vortex line in superfluid ^4He : Effects of gauge-symmetry breaking, *Phys. Rev. B* **49**, 12381 (1994).
15. G. Baym and E. Chandler, The hydrodynamics of rotating superfluids. I. zero-temperature, nondissipative theory, *J. Low Temp. Phys.* **50**, 57 (1983).
16. V. D. Fil, T. V. Ignatova, N. G. Burma, A. I. Petrishin, D. V. Fil, and N. Yu. Shitsevalova, Mass of an Abrikosov vortex, *Low Temp. Phys.* **33**, 1019 (2007).
17. D. Golubchik, E. Polturak, and G. Koren, Mass of a vortex in a superconducting film measured via magneto-optical imaging plus ultrafast heating and cooling, *Phys. Rev. B* **85**, 060504 (2012).
18. N. B. Kopnin and V. M. Vinokur, Dynamic vortex mass in clean Fermi superfluids and superconductors, *Phys. Rev. Lett.* **81**, 3952 (1998).
19. N. B. Kopnin and V. E. Kravtsov, Conductivity and Hall effect of pure type-II superconductors at low temperatures, *Pis'ma Zh. Eksp. Teor. Fiz.* **23**, 631 [*JETP Lett.* **23**, 578] (1976).
20. R. Tesař, M. Šindler, J. Koláček, and L. Skrbek, Terahertz wire-grid circular polarizer tuned by lock-in detection method, *Rev. Sci. Instrum.* **89**, 083114 (2018).
21. R. Tesař, Z. Šimša, J. Koláček, M. Šindler, L. Skrbek, K. Il'in, and M. Siegel, Terahertz transmission of NbN superconductor thin film, *Physica C* **470**, 932 (2010).
22. R. Liang, D. A. Bonn, and W. N. Hardy, Evaluation of CuO_2 plane hole plane hole doping in $\text{YBa}_2\text{Cu}_3\text{O}_{6+x}$ single crystals, *Phys. Rev. B* **73**, 180505(R) (2006).
23. N. Blumenschein, C. Kadlec, O. Romanyuk, T. Paskova, J. F. Muth, and F. Kadlec, Dielectric and conducting properties of unintentionally and Sn-doped $\beta\text{-Ga}_2\text{O}_3$ studied by terahertz spectroscopy, *J. Appl. Phys.* **127**, 165702 (2020).
24. E. B. Sonin, *Dynamics of Quantised Vortices in Superfluids*, Cambridge University Press (2016).
25. U. Welp, W. K. Kwok, G. W. Crabtree, K. G. Vandervoort, and J. Z. Liu, Magnetic measurements of the upper critical field of $\text{YBa}_2\text{Cu}_3\text{O}_{7-\delta}$ single crystals, *Phys. Rev. Lett.* **62**, 1908 (1989).
26. M. Šindler, R. Tesař, J. Koláček, P. Szabó, P. Samuely, V. Hašková, C. Kadlec, F. Kadlec, and P. Kužel, *Supercond. Sci. Technol.*, **27**, 055009 (2014).
27. F. Kadlec, C. Kadlec, J. Vít, F. Borodavka, M. Kempa, J. Prokleška, J. Buršík, R. Uhrecký, S. Rols, Y. S. Chai, K. Zhai, Y. Sun, J. Drahokoupil, V. Goian, and S. Kamba, Electromagnon in the Z -type hexaferrite $(\text{Ba}_x\text{Sr}_{1-x})_3\text{Co}_2\text{Fe}_{24}\text{O}_{41}$, *Phys. Rev. B*, **94**, 024419 (2016).
28. B. Parks, S. Spielman, J. Orenstein, D. T. Nemeth, F. Ludwig, J. Clarke, P. Merchant, and D. J. Lew, Phase-sensitive measurements of vortex dynamics in the terahertz domain, *Phys. Rev. Lett.* **74**, 3265 (1995).
29. Š. Višňovský, *Optics in Magnetic Multilayers and Nanostructures* (CRC Press, 2006).
30. Supplementary Information
31. N. B. Kopnin and V. M. Vinokur, Superconducting Vortices in ac Fields: Does the Kohn Theorem Work?, *Phys. Rev. Lett.* **87**, 017003 (2001).

32. E. B. Sonin, Interaction of ultrasound with vortices in type-II superconductors, Phys. Rev. Lett. **76**, 2794 (1996).
33. P.-J. Lin and P. Lipavský and P. Matlock, Inertial Josephson relation for FIR frequencies, Phys. Lett. A **376**, 883 (2012).
34. J. I. Gittleman and B. Rosenblum, Radio-Frequency Resistance in the Mixed State for Subcritical Currents, Phys. Rev. Lett. **16**, 734 (1966).

Acknowledgements

We thank Chih-Wei Luo for preparing the YBaCuO sample and for providing the temperature dependence of dc resistivity. The authors are grateful to E. B. Sonin for his kind help with the finite-frequency modification of the equation of vortex motion and to T. Simula and G. E. Volovik for valuable comments. We acknowledge the support of the Czech Science Foundation (project No. 21-11089S), P. L. that of INTER-EXCELLENCE (COST) LTC 18024, C. K. SOLID21-CZ.02.1.01/0.0/0.0/16 019/0000760 and L. S. thanks the Czech Science Foundation (project No. 20-00918S).

Author contributions statement

J.K. designed the experiment; R.T. developed the circular polarizer and built the experimental setup; R.T. and M.Š. performed the measurement of dichroism; C.K. performed the time-domain THz measurements; P.L., M.Š., L.S., and J.K. analyzed the results. All authors contributed to the discussions and production of the manuscript.

Additional information

The authors declare no competing interests.

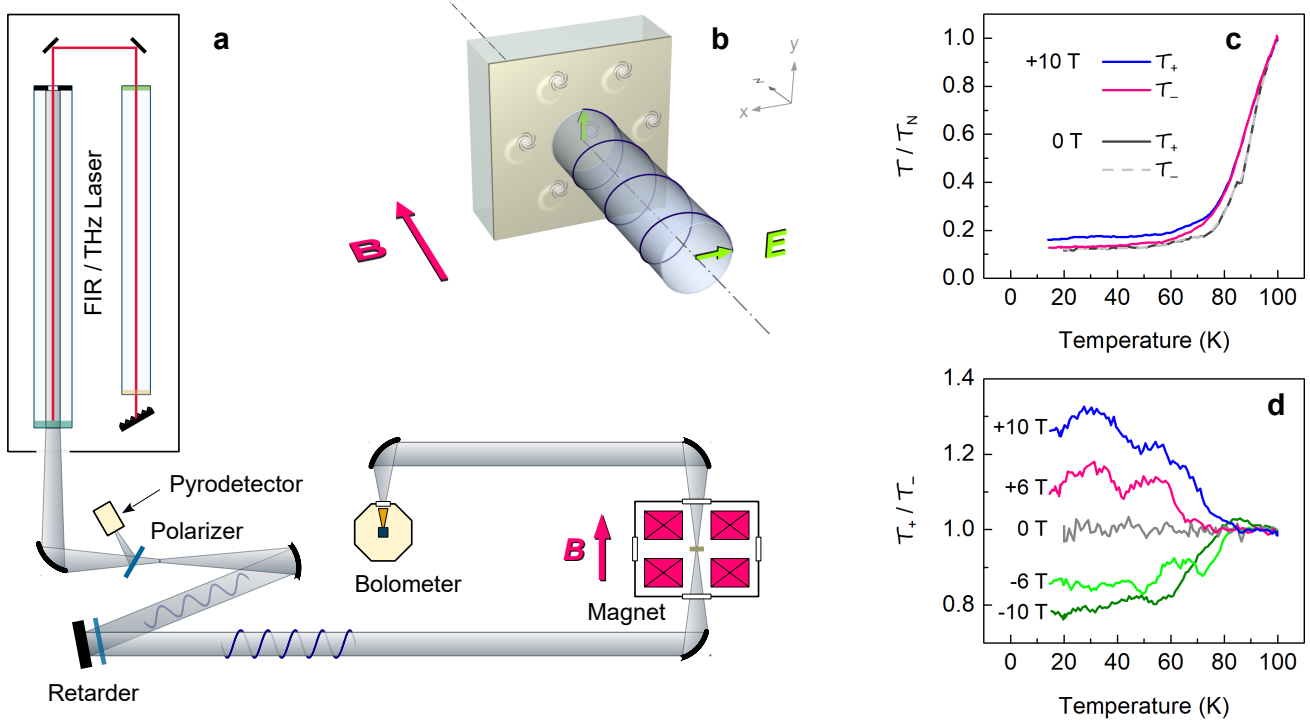


Figure 1. Far-infrared measurement of fluxon mass. **(a)** Sketch of the magneto-optical setup. The continuous laser beam is split by a linear wire-grid polarizer; the reflected part is monitored using a pyroelectric detector to keep trace of unavoidable power fluctuations, whereas the transmitted part proceeds toward the sample. The retarder converts the light from linear to circular polarization. The propagation of the circularly polarized beam and the magnetic field are perpendicular to the film surface, as detailed in panel b. **(b)** Vortices in the film (gray circles) control the transmittance of the sample via the following mechanism: The electric field of the laser light drives the supercurrent. The Magnus force accelerates vortices in the direction perpendicular to the supercurrent; in reaction, the vortex motion affects the supercurrent and, thus, the transmittance. In the sketch, the electric field in the sample, as well as the vortices, rotate clockwise. If the light frequency is close to the cyclotron frequency of vortices, the motion of vortices is resonantly enhanced, leading to the observed dichroism. The extent of the cyclotron motion is strongly exaggerated; in fact, the fluxon circulates on a radius of less than 10^{-12} m at the strongest laser line. **(c)** Transmittance of the $\text{YBa}_2\text{Cu}_3\text{O}_{7-\delta}$ superconducting sample, normalized to the normal-state transmittance \mathcal{T}_N at 100 K and plotted for two circular polarizations versus temperature. The dichroism is clearly visible below 70 K in a magnetic field of 10 T; in a zero field, no dichroism appears. **(d)** Transmittance ratio $\mathcal{T}_+/\mathcal{T}_-$ measured in several applied magnetic fields plotted versus temperature. The data were obtained using a $312 \mu\text{m}$ laser line (6.1×10^{12} rad/s). Above the critical temperature, the dichroism is absent, showing that the normal-state Hall component is negligible.

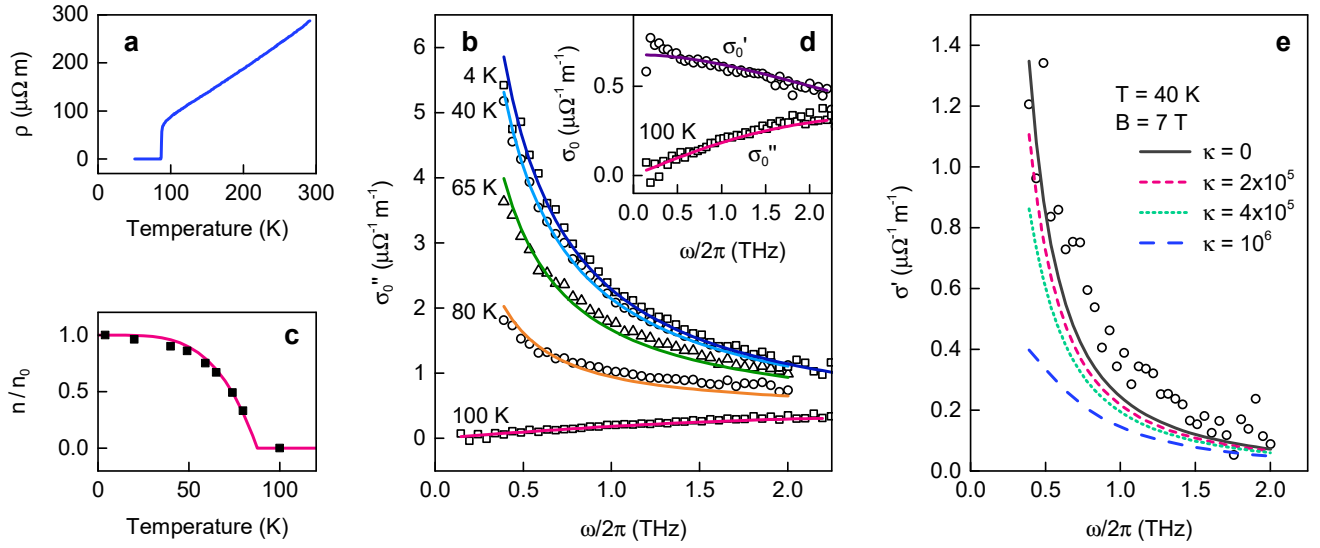


Figure 2. Sample specification. Panels a–d refer to zero magnetic field. (a) The dc resistivity as a function of temperature provides the critical temperature $T_c = 87.6$ K. Extrapolation of the normal-state resistivity below T_c gives negligible residual resistivity. (b) The imaginary part of the conductivity as a function of frequency for several temperatures. The two-fluid model (lines) reproduces the data (symbols) for the superconducting fraction $f_s = 1 - T^4/T_c^4$ (line) compared in (c) with fitted values. (d) The real (circles) and imaginary (squares) conductivities at 100 K provide the relaxation time $\tau_N = 47$ fs. (e) The measured real part of conductivity for linearly polarized light at magnetic field 7 T (circles) compared with fits based on the vortex dynamics, $\sigma = \frac{1}{2}(\sigma_+ + \sigma_-)$, supports small pinning with $\kappa = 2 \times 10^5$ N/m².

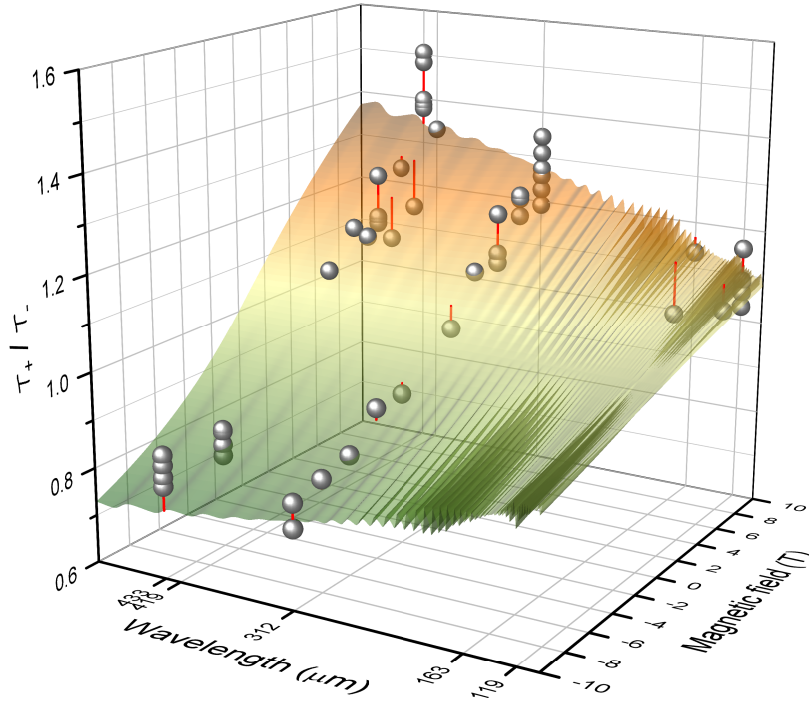


Figure 3. Transmittance ratio $\mathcal{T}_+/\mathcal{T}_-$ for the laser lines 119, 163, 312, 419, and 433 μm as a function of magnetic field. The theoretical prediction (colored surface) with no free fitting parameter is compared with experimental values (spheres) observed at a temperature of 45 K. The corrugation of the theoretical surface results from interference in the film/substrate structure. Its amplitude is smaller than the experimental error. The values observed under identical conditions but in different runs hang on the same vertical line attached to the surface. These repeated measurements demonstrate a spread of the experimental data. Despite the experimental uncertainty, the overall magnitude and dependence on magnetic field and wavelength are consistent with the Kopnin-Vinokur theory.

Supplementary Information

Mass of Abrikosov vortex in high-temperature superconductor $\text{YBa}_2\text{Cu}_3\text{O}_{7-\delta}$

Roman Tesař, Michal Šindler, Christelle Kadlec, Pavel Lipavský, Ladislav Skrbek, and Jan Kolářek

Calculation of transmittance

Our sample comprised a thin YBaCuO film with a thickness of $L = 107$ nm, deposited on a lanthanum aluminate (LAO) substrate. Anisotropic properties of the substrate were measured with standard time-domain THz spectroscopy. For convenience, the x -axis was chosen parallel to the linear polarization of the ordinary ray. At a low temperature of 20 K, we established the substrate thickness $D = 513.5$ μm and dispersion of ordinary and extraordinary refractive indices shown in Figure S1. Measurements at temperatures up to 100 K did not reveal any appreciable deviation from the low-temperature values.

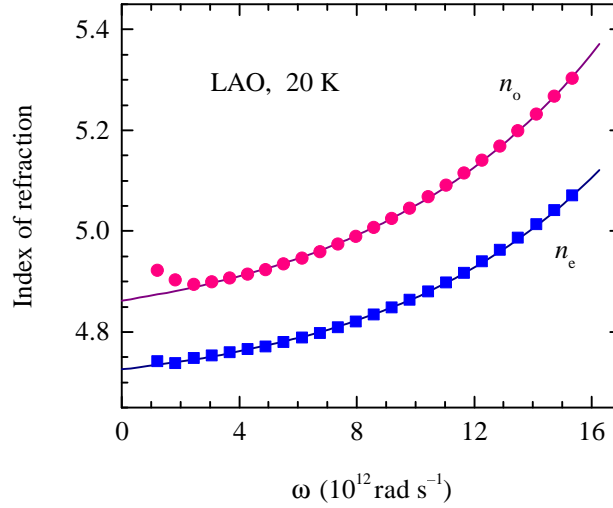


Figure S1. Ordinary (n_o) and extraordinary (n_e) refractive index of lanthanum aluminate (LAO) substrate measured at a temperature of 20 K. The frequency dependence is well described by exponential functions $n_o = 4.789 + 0.073 \exp(0.127\omega)$ and $n_e = 4.675 + 0.051 \exp(0.134\omega)$ with the angular frequency ω in 10^{12} rad/s units (solid lines).

When calculating the sample transmittance, it is necessary to combine two different approaches. Circular dichroism in YBaCuO is naturally described within a vector basis related to the circular polarization of the laser beam. On the other hand, the birefringence of the substrate is conveniently represented in a linear basis associated with the anisotropy axes of LAO. To match these two basis we employ Yeh's 4×4 matrix algebra¹⁻⁴.

In each of the segments, vacuum| YBaCuO |LAO|vacuum, we write the resulting electric field $\mathbf{E}(z, t) = \mathbf{E}(z)e^{-i\omega t}$ as a sum of four partial waves^{1,3}

$$\mathbf{E}(z) = \sum_{j=1}^4 E_j \mathbf{e}_j e^{ik_j z}, \quad (\text{S1})$$

where \mathbf{e}_j stand for eigen-polarization vectors and k_j for wavevectors. Partial waves propagating forward are indexed by odd numbers $j = 1, 3$ and waves propagating backward by even numbers $j = 2, 4$. In vacuum and YBaCuO , the eigen-polarization vectors \mathbf{e}_j are given in the helical basis as $\mathbf{e}_{1,3} = \mathbf{e}_{2,4} = (\mathbf{x} \pm i\mathbf{y})/\sqrt{2}$. In LAO, we use the linear basis $\mathbf{e}_{1,2} = \mathbf{x}$ and $\mathbf{e}_{3,4} = \mathbf{y}$. Now we collect the amplitudes E_j of partial waves into a four-component column vector and express the light propagation in a matrix form as

$$\mathbf{E}_{in} = \mathbf{M}\mathbf{E}_{tr}, \quad (\text{S2})$$

where the 4×4 transfer matrix

$$\mathbf{M} = \mathbf{D}_{\text{vac}}^{-1} \mathbf{D}_{\text{film}} \mathbf{P}_{\text{film}} \mathbf{D}_{\text{film}}^{-1} \mathbf{D}_{\text{subs}} \mathbf{P}_{\text{subs}} \mathbf{D}_{\text{subs}}^{-1} \mathbf{D}_{\text{vac}} \quad (\text{S3})$$

connects the incident electric field with the transmitted one via a sequence of dynamical and propagation matrices. The propagation matrices are diagonal. For the YBaCuO film, we have $(\mathbf{P}_{\text{film}})_{ij} = \delta_{ij} e^{ik_j L}$ with $k_{1,2} = \pm n_+ \omega/c$ and $k_{3,4} = \pm n_- \omega/c$, where c is the vacuum speed of light and

$$n_{\pm} = \sqrt{\frac{i\sigma_{\pm}}{\omega\varepsilon_0}} \quad (\text{S4})$$

is the complex refractive index related to the complex circular conductivity σ_{\pm} . Similarly, for the LAO substrate, $(\mathbf{P}_{\text{subs}})_{ij} = \delta_{ij} e^{iq_j D}$ with $q_{1,2} = \pm n_o \omega/c$ and $q_{3,4} = \pm n_e \omega/c$. Matching of electromagnetic waves at segment interfaces is covered by dynamical matrices

$$\mathbf{D}_{\text{vac}} = \frac{1}{\sqrt{2}} \begin{pmatrix} 1 & 1 & 1 & 1 \\ 1 & -1 & 1 & -1 \\ i & i & -i & -i \\ -i & i & i & -i \end{pmatrix}, \quad \mathbf{D}_{\text{film}} = \frac{1}{\sqrt{2}} \begin{pmatrix} 1 & 1 & 1 & 1 \\ n_+ & -n_+ & n_- & -n_- \\ i & i & -i & -i \\ -in_+ & in_+ & in_- & -in_- \end{pmatrix}, \quad (\text{S5})$$

$$\mathbf{D}_{\text{subs}} = \begin{pmatrix} 1 & 1 & 0 & 0 \\ n_o & -n_o & 0 & 0 \\ 0 & 0 & 1 & 1 \\ 0 & 0 & -n_e & n_e \end{pmatrix}.$$

As already mentioned, we use the same helical basis for vacuum and YBaCuO, which leads to a similarity of \mathbf{D}_{vac} and \mathbf{D}_{film} . Since no light approaches the sample from its backside, $(\mathbf{E}_{tr})_2 = 0$ and $(\mathbf{E}_{tr})_4 = 0$, we obtain the transmittances of circularly polarized light in the form

$$\begin{aligned} \mathcal{T}_+ &= (|M_{33}|^2 + |M_{31}|^2) S, \\ \mathcal{T}_- &= (|M_{13}|^2 + |M_{11}|^2) S, \end{aligned} \quad (\text{S6})$$

where $S = |M_{11}M_{33} - M_{13}M_{31}|^{-2}$ is a submatrix determinant. The superposition of partial waves in the substrate leads to strong oscillations with the wavelength (see Fig. S2a). These interference effects, however, are considerably reduced in the ratio of transmittances with opposite helicity

$$\frac{\mathcal{T}_+}{\mathcal{T}_-} = \frac{|M_{33}|^2 + |M_{31}|^2}{|M_{13}|^2 + |M_{11}|^2}, \quad (\text{S7})$$

as documented in Fig. S2b.

For purposes of discussion, we can use a free-film approximation which is obtained by sending the substrate thickness to zero, $D \rightarrow 0$. A further simplification follows from the expansion in the film thickness according to Hooper and Sambles⁵,

$$\frac{1}{\mathcal{T}} = 1 + \frac{\sigma'}{\varepsilon_0 \omega} \left(\frac{L\omega}{c} \right) + \frac{|\sigma|^2}{4\varepsilon_0^2 \omega^2} \left(\frac{L\omega}{c} \right)^2 + \frac{\sigma' \sigma''}{3\varepsilon_0^2 \omega^2} \left(\frac{L\omega}{c} \right)^3 + \frac{1}{12} \left[2 \frac{|\sigma|^2}{\varepsilon_0^2 \omega^2} + \frac{\sigma''}{\varepsilon_0 \omega} + \frac{\sigma'' |\sigma|^2}{(\varepsilon_0 \omega)^3} \right] \left(\frac{L\omega}{c} \right)^4, \quad (\text{S8})$$

adapted to our notation by substituting for permittivity $\varepsilon = 1 + i\sigma/(\varepsilon_0 \omega)$. This expansion is nearly exact but still too complicated. Numerical calculations reveal that the third term is dominant in our case

$$\mathcal{T} \approx \frac{4\varepsilon_0}{\mu_0 L^2 |\sigma|^2}. \quad (\text{S9})$$

We used the approximation (S9) in the main text to discuss the observed dichroism

$$\frac{\mathcal{T}_+}{\mathcal{T}_-} \approx \frac{|\sigma_-|^2}{|\sigma_+|^2}. \quad (\text{S10})$$

Its validity is demonstrated in Fig. S2b.

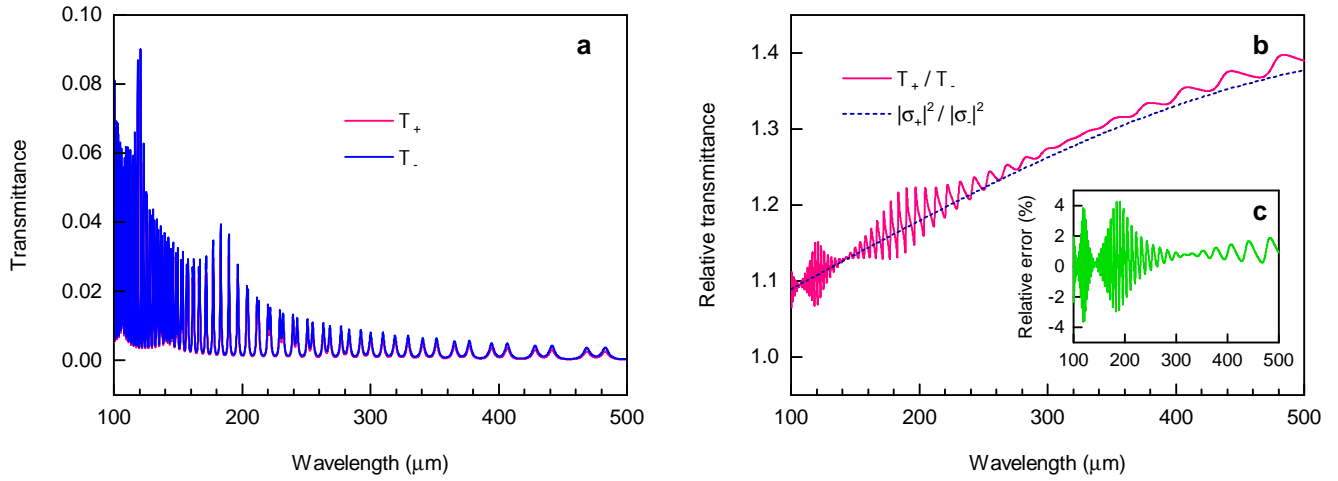


Figure S2. Transmittance as a function of the laser wavelength for $B = 10$ T and $T = 45$ K. **(a)** Interference in the sample substrate leads to strong oscillation in the transmittance. Due to weak birefringence of the substrate, both circular polarizations follow similar but not identical pattern. **(b)** The interference almost cancels in the ratio of transmittances (red line). The free-film approximation (blue line) differs from the exact result by less than 4%, as detailed in the inset **(c)**.

References

1. Yeh, P., Electromagnetic propagation in birefringent layered media, *J. Opt. Soc. Am.* **69**, 742 (1979).
2. Yeh, P., Optics of anisotropic layered media: A new 4×4 matrix algebra, *Surf. Sci.* **96**, 41 (1980).
3. Višňovský, Š., *Optics in Magnetic Multilayers and Nanostructures* (CRC Press, 2006).
4. Šindler, M., Tesař, R., Koláček, J., and Skrbek, L., Interpretation of transmission through type-II superconducting thin film on dielectric substrate as observed by laser thermal spectroscopy, *Physica C* **483**, 127 (2012).
5. I. R. Hooper, and J. R. Sambles, Some considerations on the transmissivity of thin metal films, *Opt. Express* **16**, 17258 (2008).